IEEE Photonics Journal
An IEEE Photonics Society Publication

Open Access

Resolution-Enhancement for an Integral Imaging Microscopy Using Deep Learning

Volume 11, Number 1, February 2019

Ki-Chul Kwon
Ki Hoon Kwon
Munkh-Uchral Erdenebat
Yan-Ling Piao
Young-Tae Lim
Min Young Kim
Nam Kim

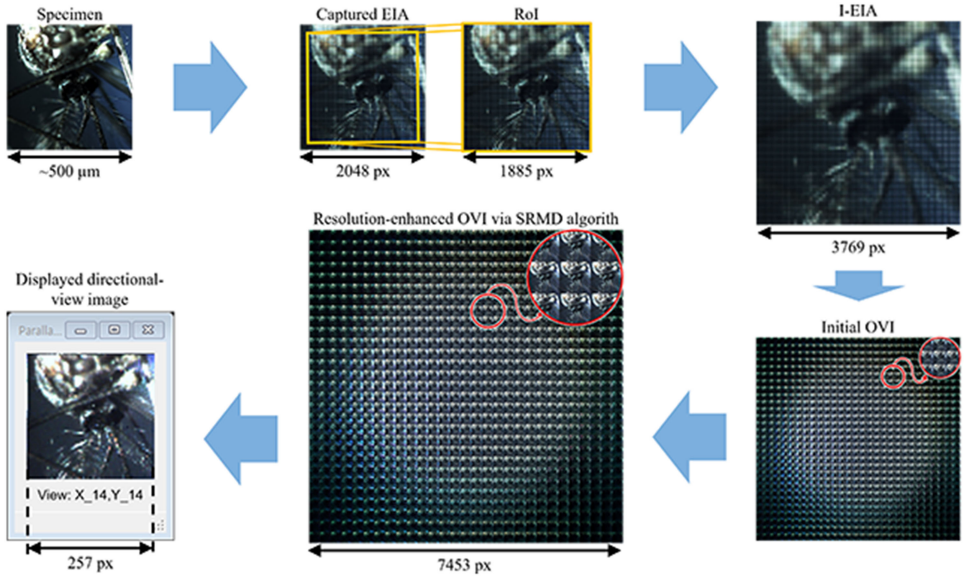

DOI: 10.1109/JPHOT.2018.2890429
1943-0655 © 2018 IEEE

Resolution-Enhancement for an Integral Imaging Microscopy Using Deep Learning

Ki-Chul Kwon,[1] **Ki Hoon Kwon**,[2] **Munkh-Uchral Erdenebat**,[1] **Yan-Ling Piao**,[1] **Young-Tae Lim**,[1] **Min Young Kim**,[2, 3] **and Nam Kim** [1]

[1]School of Information and Communication Engineering, Chungbuk National University, Chungbuk 28644, South Korea
[2]School of Electronics Engineering, Kyungpook National University, Daegu 41566, South Korea
[3]Research Center for Neurosurgical Robotic System, Kyungpook National University, Daegu 41566, South Korea

DOI:10.1109/JPHOT.2018.2890429

Manuscript received November 23, 2018; revised December 20, 2018; accepted December 26, 2018. Date of publication January 1, 2019; date of current version January 15, 2019. This work was supported in part by the Institute for Information and Communications Technology Promotion (2016-0-00564, Development of Intelligent Interaction Technology Based on Context Awareness and Human Intention Understanding, under support program IITP-2018-2015-0-00448) and in part by the National Research Foundation of Korea (NRF) (no. NRF-2018R1D1A3B07044041) grant funded by the Korea Government. Corresponding authors: Nam Kim and Min Young Kim (e-mail: namkim@chungbuk.ac.kr; minykim@knu.ac.kr).

Abstract: A novel resolution-enhancement method for an integral imaging microscopy that applies interpolation and deep learning is proposed, and the complete system with both hardware and software components is implemented. The resolution of the captured elemental image array is increased by generating intermediate-view elemental images between each neighboring elemental image, and an orthographic-view visualization of the specimen is reconstructed. Then, a deep learning algorithm is used to generate maximum possible resolution for each reconstructed directional-view image with improved quality. Since a pre-trained model is applied, the proposed system processes the images directly without data training. The experimental results indicate that the proposed system produces resolution-enhanced directional-view images, and quantitative evaluation methods for reconstructed images such as the peak signal-to-noise ratio and the power spectral density confirm that the proposed system provides improvements in image quality.

Index Terms: Deep learning, integral imaging microscopy, resolution enhancement.

1. Introduction

An optical microscope is a piece of equipment that helps to enlarge very small objects that cannot be observed in detail with the human eye, through a microscopic (objective) lens. Optical microscopes are widely used, especially in biomedical research and educational applications, and various resolution enhancement methods have been proposed [1], [2]. Although a conventional microscope enlarges the image of the specimen, the observer can only see a two-dimensional (2D) representation, and depth and parallax information cannot be visualized. In recent years, several types of three-dimensional (3D) optical microscope systems, such as stereoscopic, confocal, digital holographic and light field microscopes, have been suggested [3]–[9]. Among these, the 3D light field/integral imaging microscopy (IIM) can acquire full 3D information on the specimen, including

parallax and depth information, through a micro lens array (MLA) and incoherent illumination; and a true-color natural 3D visualization of the specimen can be reconstructed [6]–[9].

Several methods have been proposed for improvement of the depth-of-field, including the spatial multiplexing method [10], a bifocal MLA recorded onto a holographic optical element [11], and a switchable bifocal liquid-crystalline polymer-dispersed MLA [12]. However, these methods do not assist in improving the resolution. The best way to improve the resolution of the reconstructed image from an IIM is to increase the number of elemental images, i.e., elemental lenses; however, the size of each elemental lens needs to be decreased to increase the number of lenses, and this smaller size leads to loss of 3D information, especially depth-of-field information. Note that the number of elemental lenses/images define the resolution of the reconstructed image, and the resolution of single elemental image defines the number of the directional-view images; therefore, the number of elemental lenses with appropriate size is more significant than the high-resolution camera sensor.

To improve the resolution of IIM without the loss of 3D information, Y.-T. Lim *et al.* applied the MLA-shifting method to the IIM acquisition process [13]. This method successfully improves the resolution of the reconstructed images; however, it is difficult to shift the MLA on a micro scale mechanically and, hence, the captured elemental image array (EIA) cannot be perfectly matched. K.-C. Kwon *et al.* proposed a user interactive-based resolution-enhanced real-time display for IIM by using an image-space parallel processing algorithm [14]–[16] and interpolation to generate intermediate-view elemental images (IVEIs) between each neighboring elemental image in the horizontal, vertical and diagonal directions; here the resolution of the reconstructed image is determined by the number of elemental images [17]. It was verified that when the interpolation process is iterated several times, the resolution of the reconstructed image is significantly improved; however, the image quality fell off greatly because of the low resolution of the initially reconstructed images during measurement of the peak signal-to-noise ratio (PSNR). If the IVEI generation process is iterated more than twice, it is possible to obtain the desired resolution during the reconstruction process; however, this requires large computational calculations with a long processing time, and the image quality is reduced when the IVEI generation process is repeated [18].

In this paper, we propose a super-resolution enhancement of IIM system using a combination of the IVEI generation method and a super-resolution algorithm based on deep learning. First, the EIA is captured from the specimen through the conventional IIM, the IVEIs are generated between the neighboring elemental images once, and an orthographic-view image (OVI) is generated from the improved-EIA (I-EIA). After the OVI is generated, the image super-resolution algorithm using a convolutional neural network, which is a typical deep learning algorithm, enhances the resolution of each directional-view image that is a sub-image of the OVI by approximately two or four times in the horizontal and vertical directions, respectively. Conventional resolution-enhancement methods for IIM, mentioned above, have a main problem that the sharpness is degraded when the resolution is improved as more than four times. Generally, the deep learning-based super-resolution algorithms are used mainly for models that improve 2-4 times in consideration of speed and performance. Actually, it is possible to train and use a corresponding model that can improve the resolution more than four times, but it is not efficient in terms of speed and performance. Therefore, in this paper, IVEI generation and deep learning algorithms are combined: the resolution of the orthographic-view image is enhanced by two almost times (in each axis) by generating the IVEIs once, and deep learning algorithm is applied to improve image resolution by 4-8 times which has better quality than using any of these methods. The theory has been confirmed through the optical experiment. The proposed system provides improved resolution for directional-view images, with less degrade in quality observed with the previously proposed methods. Based on the proposed system, a prototype of an IIM display system using interpolation and the deep learning algorithm is implemented. Section 2 reviews the principle of the conventional IIM system, the previous IVEI generation method for IIM, and the existing super-resolution method based on deep learning, Section 3 describes the methodology, and Section 4 presents experimental results and image quality evaluations.

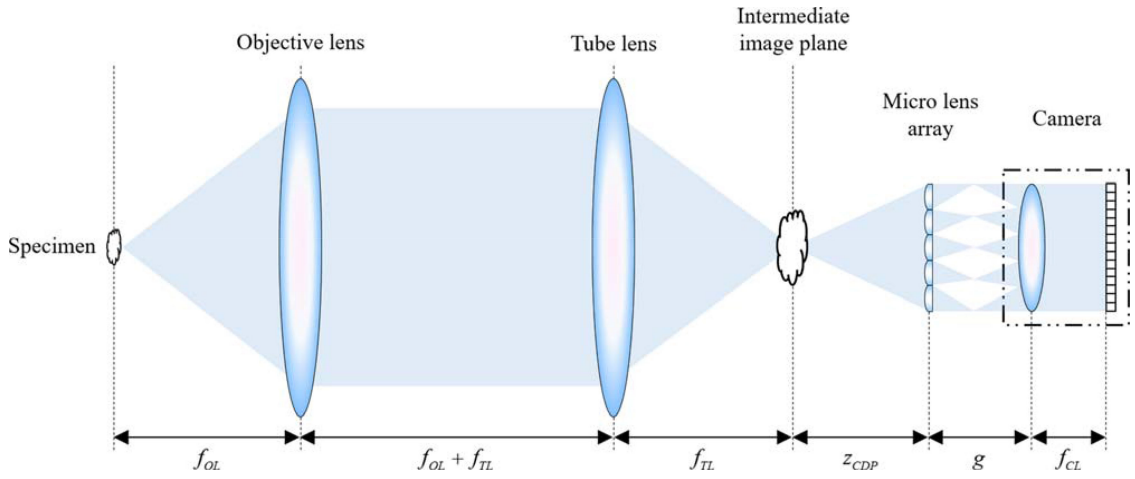

Fig. 1. Basic schematic configuration of the IIM and the geometry of the disparity between the elemental images.

2. Background

2.1 Principle for the IIM Resolution

Fig. 1 shows a schematic of the IIM and EIA capture process. The 4-*f* optical system is configured between the specimen and intermediate image plane, and a camera captures the EIA through an MLA, from the enlarged specimen at the intermediate plane. Here, the focal lengths of objective and tube lenses are given by f_{OL} and f_{TL} respectively, the distance between the intermediate image plane and MLA is set by z_{CDP}, and the camera is placed behind the MLA at a distance g. As discussed, an object point is imaged through the multiple elemental lenses in the IIM case, and is placed in different positions in each elemental image. Finally, according to the obtained disparity, the OVI is reconstructed. The resolution of each elemental image defines the number of directional-view images, and the number of captured elemental images defines the resolution of each directional-view image.

The object point with initial coordinate (x, y, z) is imaged onto the EIA plane through the (i, j)-th elemental lenses and camera lens as:

$$\begin{cases} x_{EI\,(i,j)} = \dfrac{f_{MLA} f_{CL} (i \times P_{EL} - x) - f_{CL}\, i \times P_{EL} (z - f_{MLA})}{(g - f_{MLA})(z - f_{MLA})} \\ y_{EI\,(i,j)} = \dfrac{f_{MLA} f_{CL} (j \times P_{EL} - y) - f_{CL}\, j \times P_{EL} (z - f_{MLA})}{(g - f_{MLA})(z - f_{MLA})} \end{cases}, \tag{1}$$

where f_{MLA} and f_{CL} are the focal lengths of the MLA and camera lens, respectively, i and j are the indices of an elemental lens according to the X and Y axes, and P_{EL} is the pitch of an elemental lens. Note that the camera parameters should be considered, because the camera lens affects the capture of the EIA. The fundamental disparity between the elemental images is given by:

$$\begin{cases} \Delta x_I = \dfrac{f_{MLA} f_{CL} P_{EL} (i_2 - i_1)}{(g - f_{MLA})(z - f_{MLA})} \\ \Delta y_I = \dfrac{f_{MLA} f_{CL} P_{EL} (j_2 - j_1)}{(g - f_{MLA})(z - f_{MLA})} \end{cases}, \tag{2}$$

that the different viewpoint and depth information are obtained for each image.

As discussed, it is impossible to apply any reasonable method to improve the resolution of IIM. The most appropriate way to improve the resolution of the OVI is to increase the number of elemental images, as this defines the resolution of each directional-view image. But the simple usage of MLA with a greater number of elemental lenses causes the problem of the loss of 3D information of the specimen. So, the IVEI generation-based method is the best way to improve the resolution of IIM. Also, it is possible to obtain the desired resolution of the reconstructed directional-view images, by

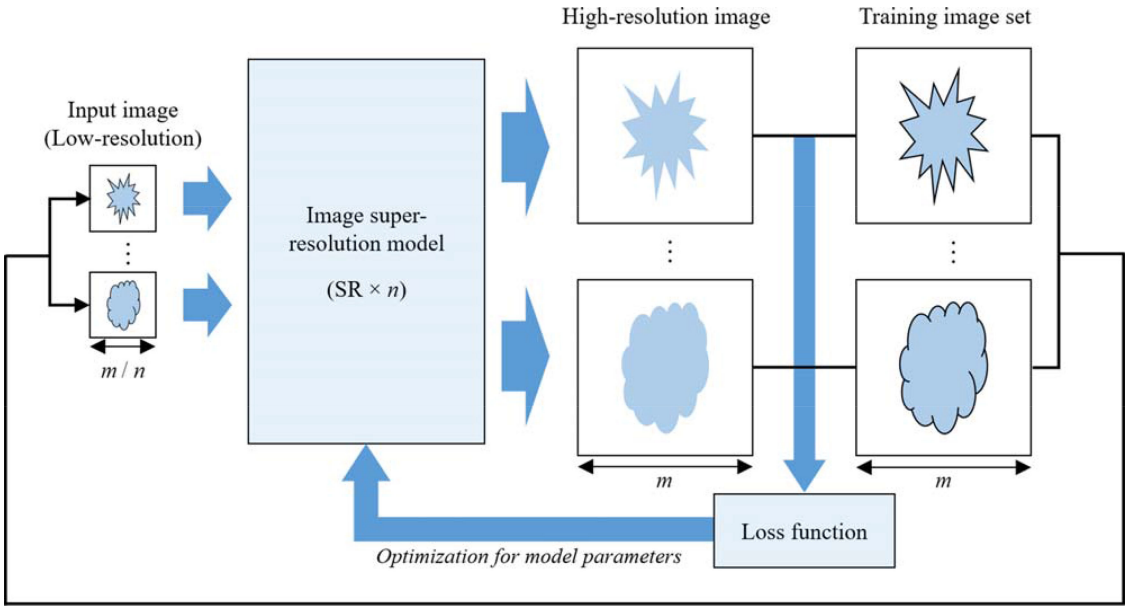

Fig. 2. Data-based model learning process for improving the image quality of low-resolution images.

repeating the IVEI generation process several times. When the IVEIs are generated more than two times repeatedly, the resolution of the directional-view images is significantly improved; however, the quality of the reconstructed image is greatly degraded through defocusing. Therefore, it is necessary to develop an IVEI generation-based resolution-enhancing method without any decrease in quality.

2.2 Super-Resolution Algorithm Based on Deep Learning

Super-resolution algorithms for improving the image quality of low-resolution images are widely used in digital image processing [19]–[24]. Among them, deep learning-based methods are highly effective for improving resolution via machine learning. As shown in Fig. 2, this kind of method learns the model for super-resolution from a large amount of training data sets. Here, first, the training data are converted into low-resolution images, and are then input into the designed learning model. Then, the error function is obtained by comparing the output high-resolution image with the input image (ground truth image) through the learning model. Finally, the optimization process for the parameters of the model is repeated to output the image closest to the original image, from the inputted low-resolution image, using the obtained error function.

Recently, the deep learning technique, which extracts and utilizes key feature information by learning through an artificial neural network, has been applied to super-resolution algorithms. In particular, convolutional neural network-based super-resolution algorithms such as SRCNN are widely used, and many improvements in super-resolution have been reported [19], [20]. Representatively, very deep super-resolution (VDSR) using a deep convolutional layer with reference to the VGG-net architecture [21], and the Laplacian pyramid super-resolution network (LapSRN), which enables progressive image super-resolution with a pyramidal model design [22], are widely used, and various other studies are underway to develop convolutional neural network-based super-resolution models. In particular, the super-resolution network for multiple degradations (SRMD), proposed by K. Zhang *et al.*, is an effective model that considers degradations such as noise in low-resolution images, unlike other convolutional neural network-based super-resolution algorithms [23].

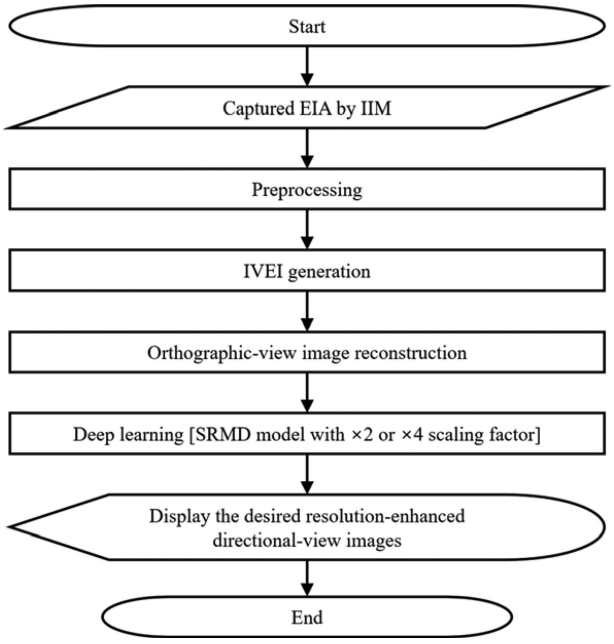

Fig. 3. Flowchart of the proposed IIM system: IIM prototype (hardware) and deep learning-based image resolution/quality enhancement (software).

3. Proposed Method

The hardware design of the proposed system is similar to the basic configuration of the IIM, as illustrated in Fig. 1. In the case of the IIM, low-quality EIAs that include degradations such as distortion and lens contamination are obtained due to the use of a poor-illumination environment and micro lenses. SRMD is currently the best method for implementing super-resolution for resolution-improvement of IIM images, because the SRMD algorithm considers the noise component in the EIA captured by IIM. So, in this paper, a novel super-resolution method for IIM reconstruction that uses the SRMD algorithm in parallel with the IVEI generation method is proposed. In addition to resolution-enhancement, the proposed system can also maintain the quality of the reconstructed directional-view images to be as similar as possible to the original image. Y. Yoon *et al.* proposed a convolutional neural network-based super-resolution method for improving the resolution of light field images [24]. The resolution of the light image was improved through end-to-end trainable architecture by cascading spatial and angular super-resolution networks; however, it is difficult to apply into IIM directly.

Fig. 3 shows a flowchart of the proposed IIM system. First, the region-of-interest (RoI) of the captured EIA is designated, and the lens distortion is corrected for the designated area. Then, the first step of resolution-enhancement, the IVEI generation method, is executed, and the resolution-enhanced OVI is reconstructed from the I-EIA. In the next step, the OVI is converted such that each directional-view image is separated to create a suitable input for deep learning. In the learning process of the super-resolution model, the resolution-enhanced OVI reconstructed from the I-EIA can cause performance degradation due its large size, so it is necessary to separate each directional-view image; these separated directional-view images are input to the learning model.

Fig. 4 shows the architecture of the convolutional super-resolution network for the SRMD model used to improve the directional-view image resolution. As mentioned above, most of the deep learning-based super-resolution algorithms are used to improve the resolution of the input image by 2-4 times. Since the deep learning-based super-resolution algorithms cannot improve the image quality with the increasing scale factor, rather it degraded the image quality, so the scale factor 2-4 are widely used. For all scale factors $n = 2$, $n = 3$ or $n = 4$, the number of convolutional layers is

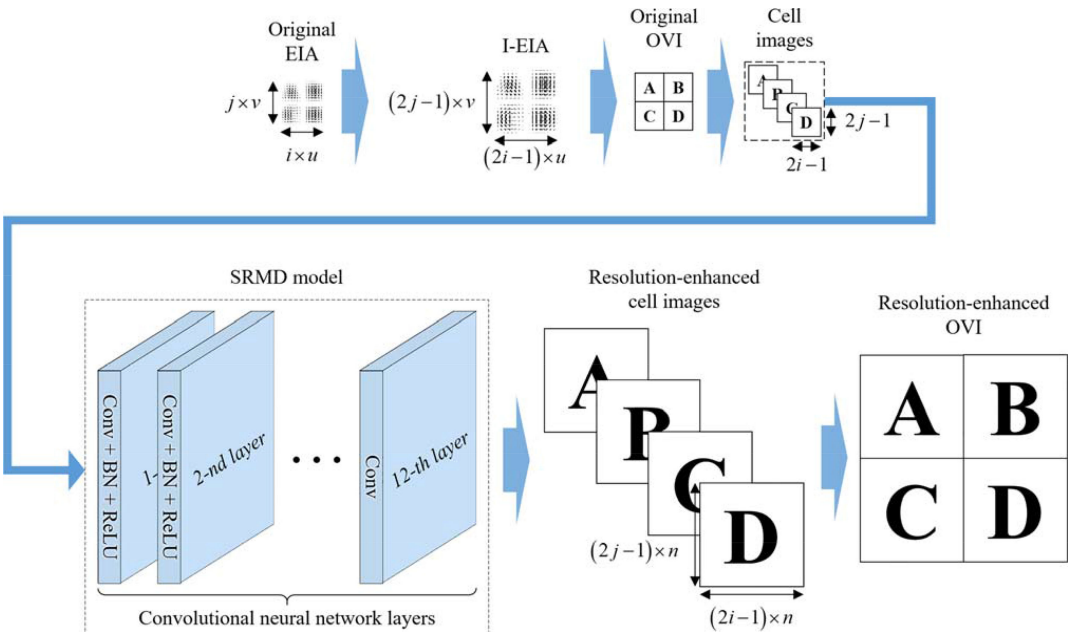

Fig. 4. Architecture of the convolutional super-resolution network applied in the proposed system.

set at 12, and the number of feature maps in each layer is set at 128. The total layer is composed of 12 layers, and each layer consists of convolution (Conv), rectified linear unit (ReLU), batch normalization (BN), and the last layer consists of only Conv. Here, the convolution operations are used for image feature extraction and analysis, and the ReLU is an activation function defined as the positive part of its argument; $f(x) = x^+ = \max(0, x)$ where x is the input to a neuron, whereby if the input value is negative, the output will be 0, and if the input value is positive, the function returns itself. BN is a technique for improving the performance and stability of artificial neural networks. It is used to normalize the input layer by adjusting and scaling the activations. The segmented images for each direction are input to the pre-trained SRMD model, which is trained in advance from a large number of image data sets in sequence with the set degradation maps. The input cell images, which are the separated directional-view images, are converted into the high-resolution images while the noises are removed simultaneously, through the layers of the SRMD model consisting of Conv, ReLU, and BN, and output.

In the proposed system, when the captured EIA includes $i \times j$ elemental images with $u \times y$ pixels each, the $u \times v$ directional-view images are reconstructed where each consists of $i \times j$ pixels. After the IVEIs are generated once, the resolution of the EIA is expanded to $[(2i-1) \times u] \times [(2j-1) \times v]$ pixels, and each directional-view image contains $(2i-1) \times (2j-1)$ pixels. Then, the scale factor of the SRMD algorithm is applied to the $\times 2$ or $\times 4$ model, according to the desired resolution by the user. Here, when the scale factor $\times 2$ model is utilized, the resolution of the output directional-view image becomes $2(2i-1) \times 2(2j-1)$, and when the $\times 4$ model is applied, the resolution of the output image will be $4(2i-1) \times 4(2j-1)$ pixels. Finally, the directional-view images are displayed on the display device and observed by the exclusive viewer, according to the user's desired viewing directions.

3. Results

3.1 System Implementation

Fig. 5(a) shows the real appearance of the proposed complex IIM system. The IIM system was designed and implemented with an MLA and a camera attached into a commercial optical micro-

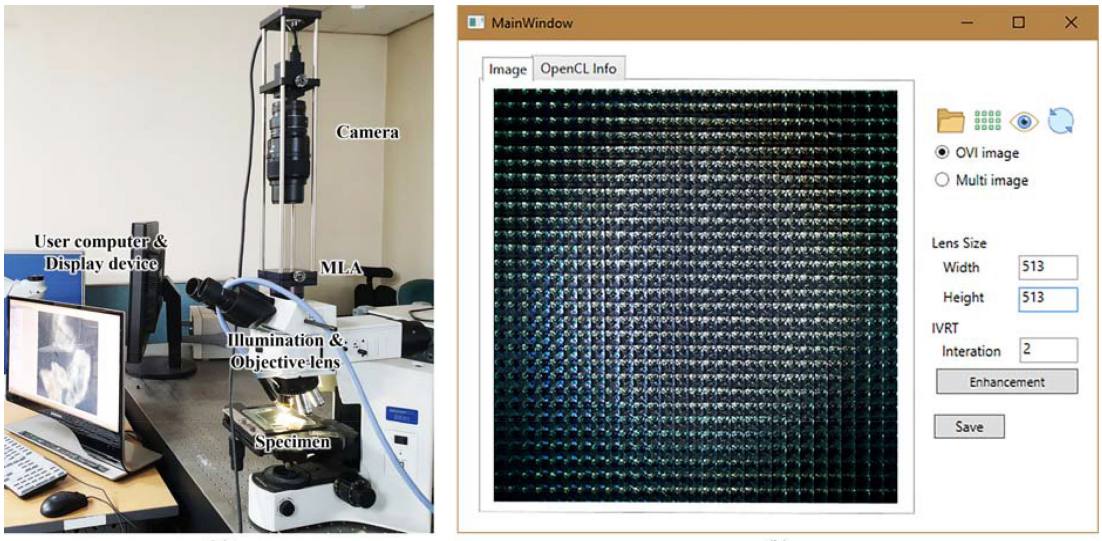

Fig. 5. (a) The prototype of the proposed IIM system: the IIM unit, user PC and display device, and (b) the user interface of viewing software for OVI and directional-view images.

TABLE 1
Specification of Implemented IIM System

Optical devices	Specifications	
IIM unit	Objective lens	×10
	Tube lens	×10
MLA	Number of lenses	100×100 lenses
	Elemental lens pitch	125 μm
	Focal length	2.4 mm
Camera	Sensor resolution	2048×2048 pixels
	Pixel pitch	5.5 μm
	Frame rate	90 fps
User PC	CPU	Intel i7-4790 3.6 GHz / 8 Cores
	Memory	16 GB
	Operating system	Windows 10 Pro (64-bit)

scope. Fig. 5(b) shows the viewing software interface for the final resolution-enhanced OVI. When the “Multi image” function is selected, the final resolution-enhanced directional-view images are displayed one-by-one, based on user interaction.

In the experiment, the Olympus BX41 microscope consisted of objective ($\times$10) and tube ($\times$10) lenses, with an MLA consisting of 100 $\times$ 100 micro lenses, each of pitch 125 μm, and a camera with a 105 mm macro lens and a 1" CMOS sensor with a resolution of 2048 $\times$ 2048 pixels, where each pixel size is 5.5 μm. The user PC has Intel i7-4790 3.6 GHz central processing unit (CPU) with 8 cores and 16 GB memory; and the pre-trained SRMD model implemented in MATLAB with MatConvNet package is utilized as a computational platform. Detailed specifications of the optical components of the IIM system and the performance of the user PC are given in Table 1.

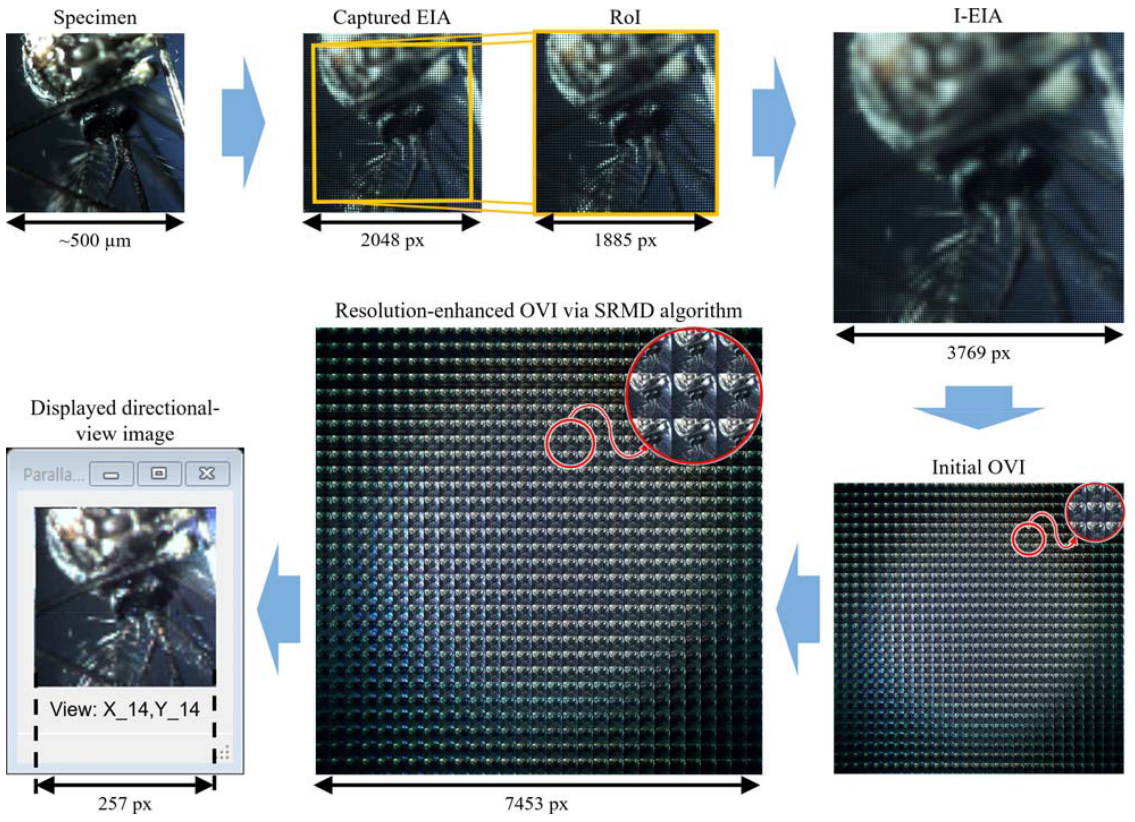

Fig. 6. Sample images at each stage of the proposed IIM system for the mosquito object.

Fig. 6 shows the corresponding images in each processing stage along the flowchart of the proposed system illustrated in Fig. 4. Here, the EIA was captured through the 100 × 100 micro lenses and camera (resolution 2048 × 2048 pixels), and the resolution of the RoI selected from the original EIA was 1885 × 1885 pixels, where the number of elemental images was 65 × 65. When the IVEIs were generated, the resolution of the EIA was improved to 3769 × 3769 pixels, and the number of elemental images was increased to 129 × 129. From the I-EIA, the OVI is reconstructed where the resolution of each directional-view image was 129 × 129 pixels.

In this paper, the SRMD method is used as a deep-learning based image super-resolution algorithm because this is the most suitable method for the proposed system. Here, the SRMD algorithm improved the resolution of directional-view images of up to 257 × 257 pixels when the scale factor n is 2, and 513 × 513 pixels when the scale factor n is 4 where the number of directional-view images was 29 × 29. Note that the improved resolution of the OVI requires more memory usage; therefore, various problems related to memory may occur. So, in the proposed system, as mentioned above, the initial directional-view images are separated and stored one-by-one, and re-combined as the resolution-enhanced OVI, after the resolution of directional-view images is improved through the SRMD algorithm. Additionally, the SRMD model was proceeded by basic CPU processing without using any parallel processing through GPU, and the processing time was measured as approximately 0.45 seconds for each directional-view image. Here, the processing time was approximately 0.43 seconds during the case of $n = 2$, and 0.46 seconds with $n = 4$ models respectively.

A total of four different specimens were acquired and reconstructed through the IIM system: a mosquito, a chip resistor, a drosophila and ore crystals. Fig. 7 shows the corresponding 2D visualizations, I-EIAs and reconstructed resolution-enhanced directional-view images for each sample with a scale factor n of 2, giving a final directional-view image of 257 × 257 pixels. An IIM

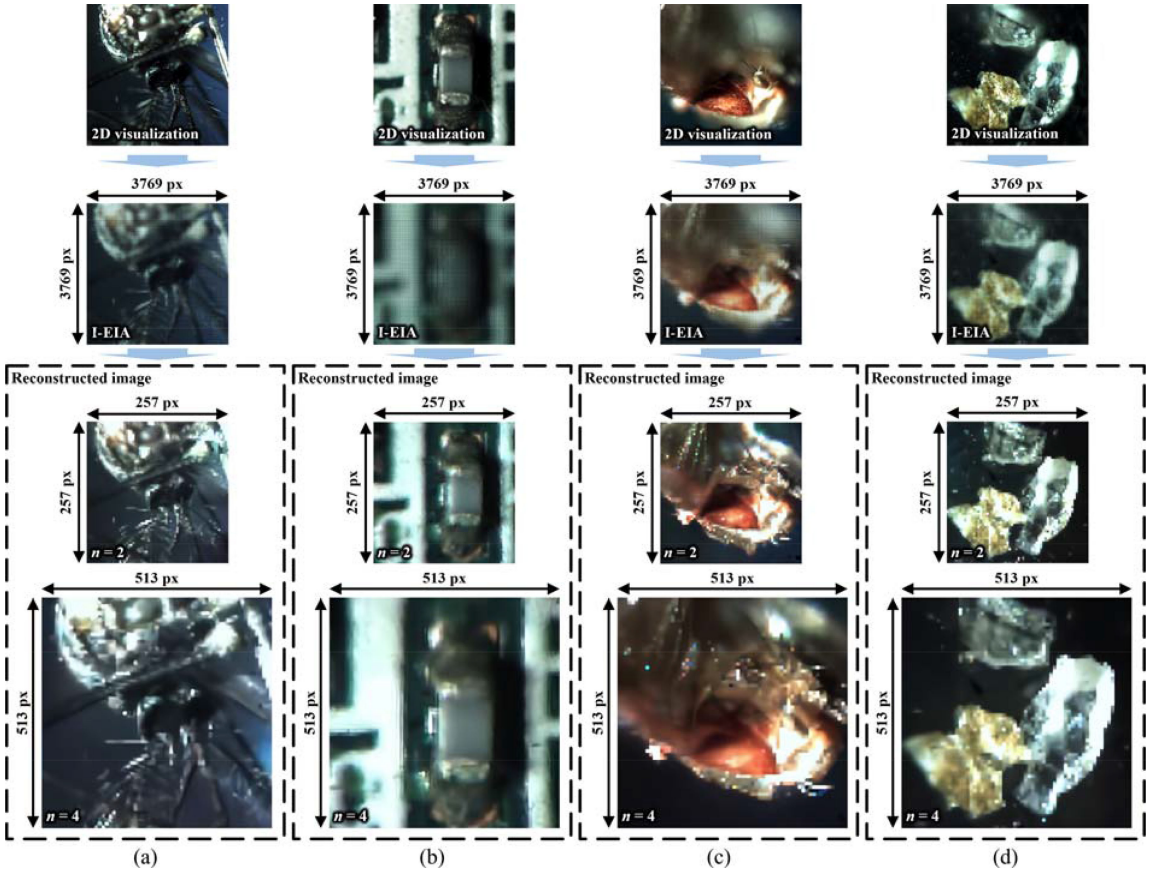

Fig. 7. The sample 2D images, I-EIAs, and reconstructed central directional-view images (view index: X_14, Y_14) for each object: (a) a mosquito (Visualization 1), (b) a chip resistor (Visualization 2), (c) a drosophila (Visualization 3), and (d) the ore crystals (Visualization 4), where scale factor n is given by 2 and 4.

system with an eightfold resolution improvement for reconstructed images is required to evaluate the resolution and quality improvements in IIM. In this experiment, it was verified that the proposed IIM system successfully improved the resolution of the directional-view images; however, a quantitative method for evaluating the enhancement in the quality of the reconstructed images was required.

3.2 Evaluation for Reconstructed Image Quality

Fig. 8 shows the displayed central directional-view images with the same view indices with Figs. 6 and 7 that is *X*_14 and *Y*_14, reconstructed from the previous iterative IVEI generation (Fig. 8(a)) and MS-LapSRN methods (Fig. 8(b)), and the proposed system (Fig. 8(c)), for each object. The quality enhancements can be observed visually, and we applied PSNR and power spectral density (PSD) measurement methods to compare the current experimental results with the previous iterative IVEI generation [18] and MS-LapSRN [22] methods, to evaluate the experimental results quantitively.

In the previous iterative IVEI generation method, the images which has been obtained by downscaling the original size of the input images repeatedly, were used as the input image, and the result images has been obtained by upscaling the corresponding input images through the iterative IVEI generation method. After the PSNR values were measured for each result image when the corresponding 2D images were set as references, it was confirmed that the PSNR values of the

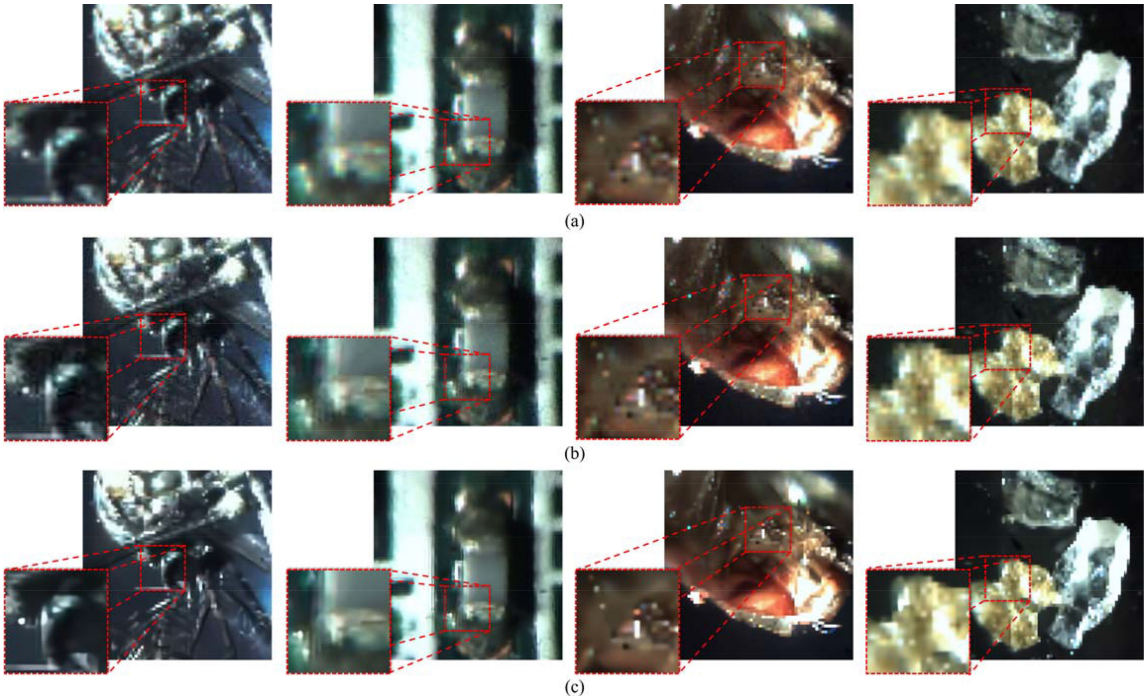

Fig. 8. Comparison between the reconstructed images from existing (a) iterative IVEI generation and (b) MS-LapSRN methods, and (c) proposed system, for four different objects where $n = 4$. Visualizations 5-12 shows the comparison between the directional-view images of central column of corresponding OVIs (view index: $X\_14, Y\_0 - X\_14, Y\_28$) which have been reconstructed though the three methods (iterative IVEI, MS-LapSRN and proposed methods), in interval of three images. Visualizations 5-8 show the case of $n = 2$, and Visualizations 9-12 show the case of $n = 4$.

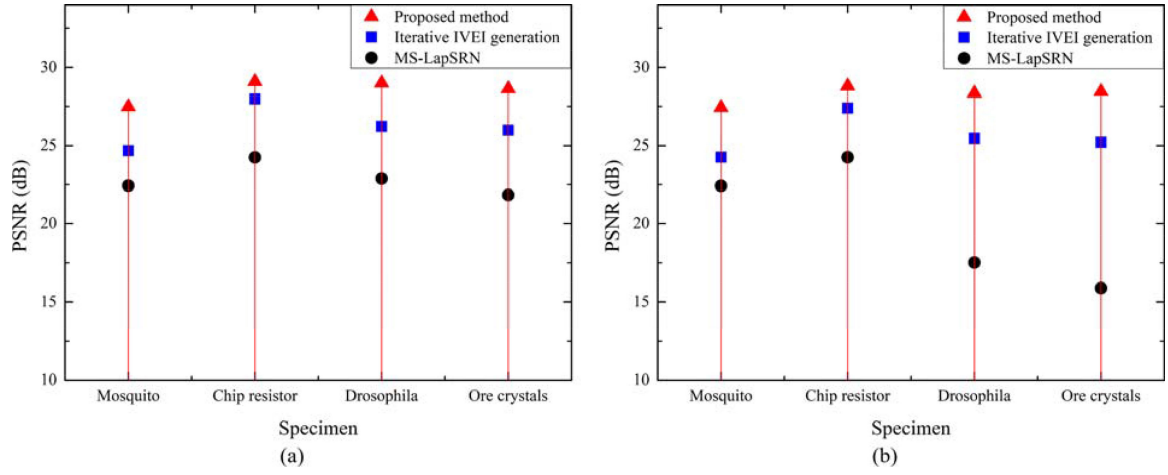

Fig. 9. Comparison between the measured PSNR values of images reconstructed via existing methods and proposed system for four different objects, in cases of (a) $n = 2$ and (b) $n = 4$ respectively.

reconstructed images have been dropped by approximately 2 −2.5 dB continuously, in each time IVEIs were generated [18].

Fig. 9 shows the PSNR measurements for the single directional-view images reconstructed using the previous iterative IVEI generation method, the conventional MS-LapSRN method and the proposed system, for scaling factors of 2 and 4, respectively. Note that, in the case of IIM, there aren't any reference images; therefore, the original directional-view images reconstructed from the initially

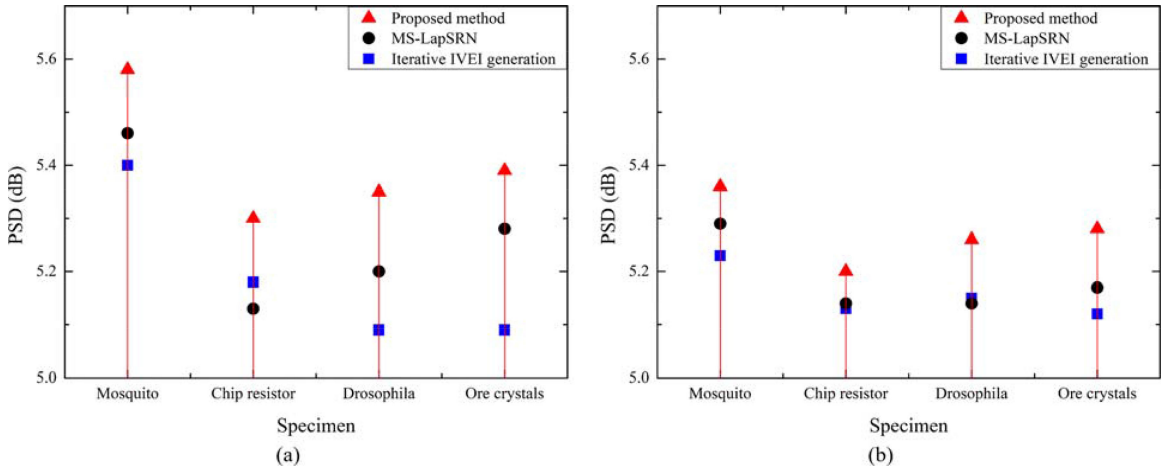

Fig. 10. Comparison of the measured PSD values of directional-view images reconstructed via existing iterative IVEI generation and MS-LapSRN methods, and proposed system for four different objects, for the cases where (a) $n = 2$ and (b) $n = 4$, respectively.

captured EIA was used as the reference, and the resolution-enhanced images reconstructed by the three methods were downscaled by the bicubic interpolation, and the PSNR values were measured. For $n = 2$, and an image resolution of 257 $\times$ 257 pixels, the PSNR values were 27.68 dB (mosquito), 29.08 dB (chip resistor), 28.99 dB (drosophila), and 28.62 dB (ore crystals) in the proposed system, while the existing methods exhibited much lower PSNR values, between 15.88 dB–27.38 dB, for the same images. A similar result was obtained for $n = 4$; the resolution of each image was 513 $\times$ 513 pixels, and the PSNR values of the directional-view images reconstructed by the proposed system using 27.43 dB (mosquito), 28.8 dB (chip resistor), 28.34 dB (drosophila), and 28.44 dB (ore crystals), while the existing methods exhibited lower values, between 15.88 dB–27.38 dB. From the PSNR measurements, it is confirmed that the proposed system improves the directional-view image resolution and produces higher quality images than previous methods, and that existing deep learning super-resolution methods such as MS-LapSRN lead to increased noise as a consequence of improving the resolution.

To measure the sharpness of the directional-view images, we measured the PSD for the reconstructed images in each case and from each object. As shown in Fig. 10(a), the PSD values were measured as 5.58 dB for the mosquito, 5.3 dB for the chip resistor, 5.35 dB for the drosophila and 5.39 dB for the ore crystals in the case of $n = 2$, while the existing methods gave 5.4 dB & 5.46 dB for the mosquito, 5.18 dB & 5.13 dB for the chip resistor, 5.09 dB & 5.2 dB for the drosophila, and 5.09 dB & 5.28 dB for the ore crystals. In the case of $n = 4$, the PSD values were measured as 5.36 dB (mosquito), 5.2 dB (chip resistor), 5.26 dB (drosophila) and 5.28 dB (ore crystals), while existing methods gave 5.23 dB & 5.29 dB (mosquito), 5.13 dB & 5.14 dB (chip resistor), 5.15 dB & 5.14 dB (drosophila) and 5.12 dB & 5.17 dB (ore crystals), respectively, as shown in Fig. 10 (b).

From the above PSNR and PSD measurements, it can be seen that the proposed system improves the resolution of reconstructed images with better quality, as compared to the conventional methods.

4. Conclusion

In this paper, we propose a novel resolution-improvement method for IIM that combines an IVEI generation method and the SRMD algorithm, which is one of the deep learning-based super-resolution methods. The EIA is captured through a conventional IIM acquisition process, and the IVEIs are generated once, after the EIA is stored. From the I-EIA, the OVI is reconstructed and each directional-view image is separated for processing. The role of the deep learning-based SRMD in

the proposed system is to configure an optimal model for resolution-improvement and image noise correction for each directional-view image. The super-resolution neural network is implemented as an SRMD model, which is a pre-learned as a general image method. We will improve the resolution of the IIM by studying the design of a new SR neural network and using the optimized IIM image as learning data.

References

[1] B. Herman and J. J. Lemasters, *Optical Microscopy: Emerging Methods and Applications*. Cambridge, MA, USA: Academic, 1985.

[2] J. Steidtner and B. Pettinger, "High-resolution microscope for tip-enhanced optical processes in ultrahigh vacuum," *Rev. Scientific Instrum.*, vol. 78, 2017, Art. no. 103104.

[3] K.-C. Kwon, Y.-T. Lim, N. Kim, K.-H. Yoo, J.-M. Hong, and G.-C. Park, "High-definition 3D stereoscopic microscope display system for biomedical applications," in *Proc. EURASIP J. Image Video Proc.*, vol. 2010, pp. 1–8, 2010.

[4] D. B. Murphy and M. W. Davidson, *Fundamentals of Light Microscopy and Electronic Imaging*, 2nd ed., Hoboken, NJ, USA:Wiley, 2012.

[5] N. Kim, M. A. Alam, L. T. Bang, A.-H. Phan, M.-L. Piao, and M.-U. Erdenebat, "Advances in the light field displays based on integral imaging and holographic techniques," *Chin. Opt. Lett.*, vol. 12, no. 6, 2014, Art. no. 06005.

[6] J.-S. Jang and B. Javidi, "Three-dimensional integral imaging of micro-objects," *Opt. Lett.*, vol. 29, no. 11, pp. 1230–1232, 2004.

[7] M. Levoy, R. Ng, A. Adams, M. Footer, and M. Horowitz, "Light field microscopy," in *Proc. SIGGRAPH*, vol. 25, pp. 924–934, 2006.

[8] J. Kim, J.-H. Jung, Y. Jeong, K. Hong, and B. Lee, "Real-time integral imaging system for light field microscopy," *Opt. Exp.*, vol. 22, no. 9, pp. 10210–10220, 2014.

[9] N. Kim and M.-U. Erdenebat, *3-D Integral Photography*, SL18. Bellingham, WA, USA:SPIE, 2016.

[10] K.-C. Kwon, M.-U. Erdenebat, M. A. Alam, Y.-T. Lim, K. G. Kim, and N. Kim, "Integral imaging microscopy with enhanced depth-of-field using a spatial multiplexing," *Opt. Exp.*, vol. 24, no. 3, pp. 2072–2083, 2016.

[11] K.-C. Kwon, Y.-T. Lim, C.-W. Shin, M.-U. Erdenebat, J.-M. Hwang, and N. Kim, "Enhanced depth-of-field of an integral imaging microscope using a bifocal holographic optical element-micro lens array," *Opt. Lett.*, vol. 42, no. 16, pp. 3209–3212, 2017.

[12] K.-C. Kwon *et al.*, "Enhancement of the depth-of-field of integral imaging microscope by using switchable bifocal liquid-crystalline polymer micro lens array," *Opti. Exp.*, vol. 25, no. 24, pp. 30503–30512, 2017.

[13] Y.-T. Lim, J.-H. Park, K.-C. Kwon, and N. Kim, "Resolution-enhanced integral imaging microscopy that uses lens array shifting," *Opt. Exp.*, vol. 17, no. 21, pp. 19253–19263, 2009.

[14] K.-C. Kwon *et al.*, "High speed image space parallel processing for computer generated integral imaging system," *Opt. Exp.*, vol. 20, no. 2, pp. 732–740, 2012.

[15] D.-H. Kim *et al.*, "Real-time 3D display system based on computer-generated integral imaging technique using enhanced ISPP for hexagonal lens array," *Appl. Opt.*, vol. 52, no. 34, pp. 8411–8418, 2013.

[16] J.-S. Jeong, K.-C. Kwon, M.-U. Erdenebat, Y. Piao, N. Kim, and K.-H. Yoo, "Development of a real-time integral imaging display system based on graphics processing unit parallel processing using a depth camera," *Opt. Eng.*, vol. 53, no. 1, 2014, Art. no. 015103.

[17] K.-C. Kwon, J.-S. Jeong, M.-U. Erdenebat, Y.-T. Lim, K.-H. Yoo, and N. Kim, "Real-time interactive display for integral imaging microscopy," *Appl. Opt.*, vol. 53, no. 20, pp. 4450–4459, 2014.

[18] K.-C. Kwon, J.-S. Jeong, M.-U. Erdenebat, Y.-L. Piao, K.-H. Yoo, and N. Kim, "Resolution-enhancement for an orthographic-view image display in an integral imaging microscope system," *Biomed. Opt. Exp.*, vol. 6, no. 3, pp. 736–746, 2015.

[19] C. Dong, C. C. Loy, K. He, and X. Tang, "Image super-resolution using deep convolutional networks," *IEEE Trans. Pattern Anal. Mach. Int.*, vol. 38, no. 2, pp. 295–307, Feb. 2016.

[20] S. Kim and H. J. Pahk, "A method for improving resolution and critical dimension measurement of an organic layer using deep learning superresolution," *Current Opt. Photon.*, vol. 2, no. 2, pp. 153–164, 2018.

[21] J. Kim, J. K. Lee, and K. M. Lee, "Accurate image super-resolution using very deep convolutional networks," in *Proc. IEEE Conf. Comput. Vision Pattern Recognit.*, 2016, pp. 1646–1654.

[22] W.-S. Lai, J.-B. Huang, N. Ahuja, and M.-H. Yang, "Fast and accurate image super-resolution with deep Laplacian pyramid networks," in *Proc. IEEE Trans. Pattern Anal. Mach. Int.*, 2018, pp. 1–13.

[23] K. Zhang, W. Zuo, and L. Zhang, "Learning a single convolutional super-resolution network for multiple degradations," in *Proc. IEEE Conf. Comput. Vision Pattern Recognit.*, 2018.

[24] Y. Yoon, H.-G. Jeon, D. Yoo, J.-Y. Lee, and I. S. Kweon, "Light-field image super-resolution using convolutional neural network," *IEEE Signal Proc. Lett.*, vol. 24, no. 6, pp. 848–852, Jun. 2017.